

Ultra-sensitive surface absorption spectroscopy using sub-wavelength diameter optical fibers

F. Warken,¹ E. Vetsch,¹ D. Meschede,¹ M. Sokolowski,² and A. Rauschenbeutel^{1,*}

¹*Institut für Angewandte Physik, Universität Bonn, 53012 Bonn, Germany*

²*Institut für Physikalische und Theoretische Chemie, Universität Bonn, 53012 Bonn, Germany*

(Dated: May 7, 2019)

The guided modes of sub-wavelength diameter air-clad optical fibers exhibit a pronounced evanescent field. The absorption of particles on the fiber surface is therefore readily detected via the fiber transmission. We show that the resulting absorption for a given surface coverage can be orders of magnitude higher than for conventional surface spectroscopy. As a demonstration, we present measurements on sub-monolayers of 3,4,9,10-perylene-tetracarboxylic dianhydride (PTCDA) molecules at ambient conditions, revealing the agglomeration dynamics on a second to minutes timescale.

PACS numbers: 78.66.Qn, 39.30.+w, 68.43.Jk, 78.66.Jg

During the last twenty years, numerous optical tools for surface and interface analysis have been developed [1]. The selective sensitivity to surface effects is often obtained by carrying out spectroscopy with evanescent waves (EW), created by total internal reflection of light at the interface. This is straightforwardly realized by exciting waveguide modes in unclad optical fibers [2, 3]. If the EW is resonant with the transition frequency of particles (atoms, molecules, quantum dots, etc.) in the surrounding medium, one can use both the particles' fluorescence [4] or the peak attenuation of the waveguide mode [2, 5] to infer the concentration of particles at the interface. Moreover, the line shapes allow to spectroscopically retrieve detailed physical information about the nature and strength of the particle-surface interaction.

Fiber-based evanescent wave spectroscopy (EWS) is used in various sensors [6]. The robustness, reliability, and ease of use of an all-fiber-based sensor technology is advantageous for in situ sensing in a remote or isolated location or in a harsh environment, e.g., in industrial applications or environmental studies. Furthermore, such sensors also profit from the multiplexing and miniaturization potential inherent to fiber technology. When measuring a volumetric concentration of particles in the surrounding medium, these sensors yield however a reduced sensitivity compared to conventional free-beam absorption: a significant fraction of the light propagates inside the waveguide and therefore does not interact with the particles of interest. This problem can partially be overcome by increasing the power fraction in the EW through proper choice of the fiber mode or geometry [7, 8, 9]. Yet, even in the ultimate case of 100 % EW, the sensitivity will not exceed that of free-beam absorption techniques.

In this letter, we demonstrate that the situation can be dramatically different when employing fiber-based EWS for the spectroscopic study of surface coverages instead of volumetric concentrations: The ultimate sensitivity of fiber-based surface absorption spectroscopy (SAS) is shown to strongly depend on the fiber diameter and to exceed free-beam SAS by several orders of magnitude in

the case of sub-wavelength diameter fibers. Fiber-based surface absorption spectroscopy (SAS) has already been used for a number of applications, e.g., in bio-sensors [10]. However, to our knowledge, these applications were only motivated by the above-mentioned practical advantages; their ultimate sensitivity was so far neither the subject of theoretical nor of experimental studies. As a demonstration, we present fiber-based SAS measurements on sub-monolayers of 3,4,9,10-perylene-tetracarboxylic dianhydride molecules (PTCDA, see inset of Fig. 3(a) below). PTCDA thin films are excellent indicators for the sensitivity because their spectral properties highly depend on the detailed arrangement of the molecules on the surface [11]. Our findings are of relevance for a large variety of fields ranging from sensorial applications in industry, environmental studies, and bio-technology to fundamental research concerning thin film growth as well as the controlled interaction of light and matter at the ultimate, microscopic scale.

We start by considering the absorbance (i.e., decadal absorption coefficient) of a dilute film of molecules deposited on a dielectric surface. It is defined as

$$\eta(\lambda) = -\lg\left(\frac{P_{\text{sig}}(\lambda)}{P_{\text{ref}}(\lambda)}\right) \approx \frac{P_{\text{abs}}(\lambda)}{\ln(10)P_{\text{ref}}(\lambda)}, \quad (1)$$

where $P_{\text{sig}}(\lambda)$ and $P_{\text{ref}}(\lambda)$ are the transmitted powers within the spectral interval $[\lambda, \lambda + \Delta\lambda]$ with and without molecules present, respectively. The right hand side of Eq. (1) holds in the limit of a weak absorption, i.e., for $P_{\text{abs}}(\lambda) = P_{\text{ref}}(\lambda) - P_{\text{sig}}(\lambda) \ll P_{\text{ref}}(\lambda)$.

The absorbance of a freely propagating light beam impinging onto the film is proportional to the surface coverage θ , i.e., the number of molecules n per surface area:

$$\eta_{\text{free}}(\lambda) = \theta\sigma(\lambda)/\ln(10), \quad (2)$$

where $\sigma(\lambda)$ is the molecules' absorption cross section. By choosing a non-zero angle of incidence ϕ , η_{free} can in principle be enhanced by a factor of $1/\cos(\phi)$. However, this factor is limited by the experimental geometry and

typically remains of order one. For free beam measurement schemes (e.g., transmission spectroscopy, differential reflection spectroscopy (DRS), or attenuated total reflection spectroscopy, see [1] for a review), the smallest detectable surface coverage is thus determined by the smallest detectable absorbance according to

$$\theta_{\min} \approx \ln(10)\eta_{\min}(\lambda)/\sigma(\lambda) . \quad (3)$$

The situation is very different in fiber-based SAS, where every molecule absorbs a constant fraction $\sigma(\lambda)/A_{\text{eff}}$ of the power with A_{eff} given by

$$A_{\text{eff}}(\lambda) = P_{\text{ref}}(\lambda)/I_{\text{surf}}(\lambda) . \quad (4)$$

A_{eff} thus corresponds to an effective area of the guided fiber mode which is normalized to the evanescent field intensity at the fiber surface, $I_{\text{surf}}(\lambda)$, calculated according to [12]. The transmitted power after interaction with n molecules is then given by

$$P_{\text{sig}}(\lambda) = P_{\text{ref}}(\lambda) [1 - \sigma(\lambda)/A_{\text{eff}}]^n , \quad (5)$$

yielding an absorbance of

$$\eta_{\text{fiber}}(\lambda) = -\lg\left(\frac{P_{\text{sig}}(\lambda)}{P_{\text{ref}}(\lambda)}\right) \approx \frac{n\sigma(\lambda)}{\ln(10)A_{\text{eff}}(\lambda)} , \quad (6)$$

where the right hand side holds for $\sigma(\lambda)/A_{\text{eff}} \ll 1$. Substituting $n = 2\pi RL\theta$, where R and L are the fiber radius and length, respectively, then yields

$$\eta_{\text{fiber}}(\lambda) \approx \frac{\theta\sigma(\lambda)}{\ln(10)} \cdot \frac{2\pi RL}{A_{\text{eff}}(\lambda)} = \eta_{\text{free}}(\lambda)\xi(\lambda) . \quad (7)$$

For a given surface coverage θ , the absorbance in fiber-based SAS is thus enhanced by a factor of $\xi(\lambda) = 2\pi RL/A_{\text{eff}}(\lambda)$. As a first estimate, we can assume $A_{\text{eff}}(\lambda) \approx \pi R^2$, yielding $\xi \approx 2L/R$. With L of the order of millimetres and R in the sub-micron range, we thus expect ξ to be as large as 10000 for typical ultra-thin fibers, promising an increase of four orders of magnitude in sensitivity. For a more rigorous estimate, we calculate $A_{\text{eff}}(\lambda)$ from Eq. (4) using the intensity profile of the fundamental guided mode of the air-clad silica fiber, see Fig. 1(a). Figure 1(b) gives $R/A_{\text{eff}}(\lambda)$ in units of $1/\lambda$ as a function of R in units of λ (red solid line). Interestingly, $R\lambda/A_{\text{eff}}(\lambda)$ reaches a maximum for $R/\lambda = 0.253$ and then rapidly goes to zero because for $R \ll \lambda$ the mode is only weakly bound and A_{eff} diverges. When seeking to detect or to characterize a given surface coverage of molecules with the highest possible sensitivity, one should thus choose a fiber radius of approximately one fourth of the central wavelength λ_c of the measured spectrum. The enhancement factor with respect to free beam spectroscopy in this case will be $\xi \approx 3.64 \times L/\lambda_c$. For $\lambda_c = 500$ nm, $\xi \approx 10000$ is, e.g., already obtained for $L = 1.5$ mm, which can easily be realized for ultra-thin optical fibers.

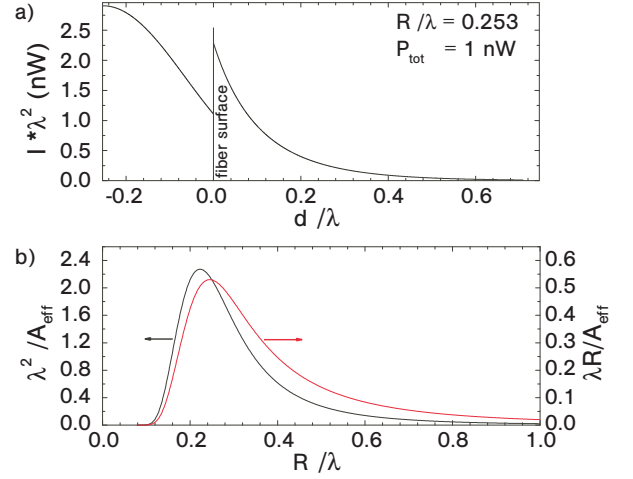


FIG. 1: (Color online) (a) Intensity profile of the fundamental guided HE_{11} mode of an air-clad silica fiber in units of Nanowatts per λ^2 as a function of the distance d from the fiber surface in units of λ . Calculated according to [12] for unpolarized light, a total guided power of 1 nW, and a fiber radius of $0.253 \times \lambda$. (b) Plot of $1/A_{\text{eff}}$ and R/A_{eff} in units of $1/\lambda^2$ and $1/\lambda$, respectively, as a function of the fiber radius R in units of λ . Assuming a refractive index of 1.46, all plots in (a) and (b) hold universally for any λ .

We note that, due to the wavelength dependence of $\xi(\lambda)$, the measured absorbance $\eta_{\text{fiber}}(\lambda)$ is not directly proportional to $\sigma(\lambda)$ as in the case of free beam spectroscopy. Before interpretation, the spectra will thus have to be normalized with respect to $\xi(\lambda)$, as calculated from Fig. 1(b). Finally, according to Eq. (6), if one seeks to detect or to characterize a given number of particles on the fiber surface rather than a given surface coverage, one will have to maximize $1/A_{\text{eff}}(\lambda)$ instead of $R/A_{\text{eff}}(\lambda)$. This is realized for a 10 % smaller fiber radius of $R/\lambda = 0.228$, see black solid line in Fig. 1(b).

In order to experimentally illustrate the enhanced sensitivity of the described method with respect to free beam measurement schemes, we have deposited PTCDA molecules on the surface of an ultra-thin fiber waist. PTCDA is an interesting model system for organic thin film growth. It forms smooth and highly ordered layers on a large variety of different substrates [13] and shows clear spectroscopic signatures for different phases [11].

We fabricate the tapered fibers by stretching a standard optical single mode fiber (Newport F-SF) while heating it with a travelling hydrogen/oxygen flame [14]. Our computer controlled fiber pulling rig produces tapered fibers with a homogeneous waist diameter down to 100 nm and a typical extension of 1–10 mm. By analytically modelling the pulling process, we can predict the resulting fiber profile with better than 10% precision. In the taper sections, the weakly guided LP_{01} mode of the unstretched fiber is adiabatically transformed into the strongly guided HE_{11} mode of the ultrathin section

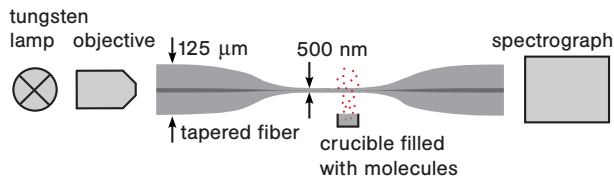


FIG. 2: (Color online) Scheme of the experimental set-up. White light from a tungsten lamp is transmitted through a tapered fiber with a 500-nm diameter waist and analyzed by a CCD spectrograph. This allows to measure the absorbance of molecules deposited on the fiber waist with a high sensitivity.

and back [15], resulting in a highly efficient coupling of light in and out of the taper waist. For monochromatic light of 850-nm wavelength and fibers with a final diameter above $0.5 \mu\text{m}$, we reach up to 97 % of the initial transmission.

A so-prepared 500-nm diameter tapered fiber with a waist length of 3 mm was used for our measurements. Figure 2 shows the simple experimental set-up, using a conventional absorption spectrometer configuration with a tungsten white light source and a commercial CCD spectrograph (Ocean Optics SW1024). A reference spectrum with 6 nm effective spectral resolution is recorded without molecules.

The molecules are deposited on the fiber waist by placing a crucible with PTCDA crystals below the fiber and by heating it up to 250°C . By convection, the air carries sublimated molecules to the fiber waist where they are adsorbed. During deposition, we continuously record spectra with an integration time of 1 s. Figure 3(a) displays a series of absorption spectra, recorded with about 25 nW of white light, not saturating the molecules. All spectra show a clear vibronic progression. Qualitatively, they agree well with DRS spectra of sub-monolayers of PTCDA on mica reported in [11]. Quantitatively, the absorbance on the high energy side is reduced by 5–10 % in our case due to the wavelength-dependance of the enhancement factor ξ . From the absorbance of 0.09–0.42 at 2.4 eV and using $\sigma = 2.7 \times 10^{-16} \text{ cm}^2$ [17] in Eq. (7), we infer that $0.5\text{--}2.3 \times 10^7$ molecules covered the fiber waist. This corresponds to a surface coverage of $1.0\text{--}4.9 \times 10^{11} \text{ cm}^{-2}$ or 0.12–0.59 % of a compact monolayer of flat lying PTCDA molecules, arranged in the herringbone structure of the (102) plane of the PTCDA bulk crystal [16]. Thus, with respect to the DRS spectra reported in [11], the smallest coverages in our case were about two orders of magnitude smaller. The strongest line at 2.42 eV (see the 1–4 s spectra) shifts by 0.02 eV to smaller energies between 4 and 53 s. This shift has been observed previously and is attributed to the condensation of isolated PTCDA molecules into two-dimensional islands [11]. This clearly demonstrates that sub-monolayer absorbance spectra can be measured very rapidly and with an excellent signal to noise ratio with fiber-based SAS.

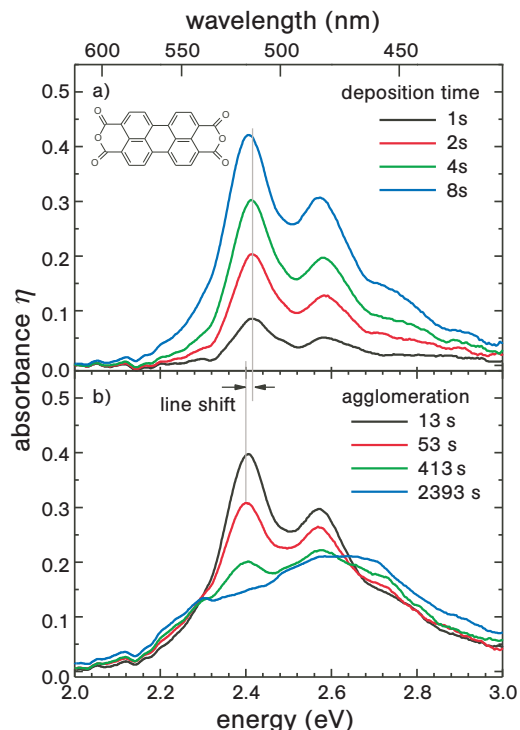


FIG. 3: (Color online) Consecutive absorbance spectra. (a) Deposition of a sub-monolayer: more and more molecules still show a monomer-like spectrum. (b) Evolution of the spectral absorption of a constant molecule number. The shape varies continuously from monomer-like to oligomer-like. Thus we observe agglomeration of the molecules on the fiber surface.

Figure 3(b) displays a series of spectra that monitor the post-deposition evolution, i.e., the ripening of the film after stopping the deposition of the molecules. We observe a continuous transformation from a monolayer to a multilayer spectrum, similar to [18]. It demonstrates that a PTCDA monolayer on a glass surface is metastable at ambient conditions and transforms into islands with a thickness of at least two monolayers within minutes. Two isosbestic points are observed at 2.30 eV and 2.67 eV, confirming that the total number of molecules is constant during the ripening.

Due to the fast data collection, we are able to extract additional kinetic details of the ripening process. In the time interval $t = 20\text{--}100$ s, our spectra can be understood as a weighted sum, $p \cdot A + (1 - p) \cdot B$, of a monolayer spectrum A (the 20 s spectrum in the inset of Fig. 4) and a spectrum B , where most PTCDA molecules have a next neighbour vertical to the glass surface and are thus dimers concerning their optical properties (the 100 s spectrum in Fig. 4). We fitted this model to our data. As an example, the 60 s spectrum and its fit are shown. The weight of the monolayer spectrum is plotted as a function of time in Fig. 4. For $t = 20\text{--}100$ s it decays with a time constant of $55(\pm 1)$ s according to an offset exponential [19], indicating first order kinetics of the ripening. We

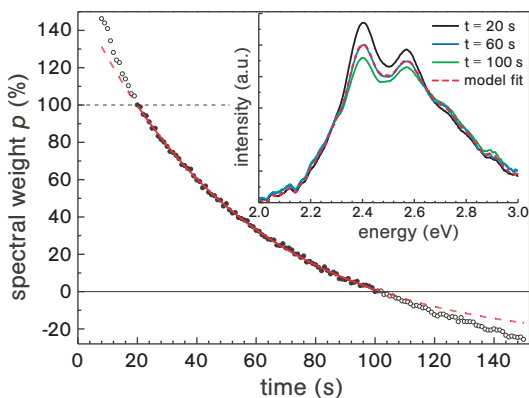


FIG. 4: (Color online) Spectral investigation of the film ripening. Spectra for $t = 20$ – 100 s can be modelled as a weighted sum of the spectra at $t = 20$ s and $t = 100$ s. As an example, we show the $t = 60$ s spectrum and the corresponding model fit (see inset). The spectral weight of the $t = 20$ s spectrum decays according to an offset exponential for $t = 20$ – 100 s [19]. The corresponding fit yields a decay constant of $55(\pm 1)$ s. The dotted line extrapolates the fit for $t < 20$ s and $t > 100$ s.

thus conclude that the molecules reorganize into dimers through a growth process rather than through two-body collisions, because the latter would lead to second order kinetics. Outside of the $t = 20$ – 100 s interval, the experimental data deviate from the extrapolated exponential behaviour (dotted line), indicating that channels other than $A \rightarrow B$ significantly contribute to the transformation dynamics. We attribute this to the above-mentioned condensation of isolated PTCDA molecules into two-dimensional islands for $t < 20$ s and to the formation of oligomers for $t > 100$ s.

Reordering of monolayer islands to a polycrystalline phase was also observed for PTCDA deposited on mica when transferring the samples from vacuum to ambient conditions [18]. The agglomeration process was however not resolved in time. By comparison with samples in a dry atmosphere, Proehl *et al.* deduced that coadsorbed water accelerates the reordering [18]. The small time constant observed in our experiment, entirely performed under ambient conditions, confirms this conclusion. Moreover, our experiment demonstrates that the metastable monolayer exists only for a very short time under ambient conditions and can hence be easily overlooked.

Summarizing, we have shown that sub-wavelength diameter optical fibers are a powerful and easy to use tool for ultra-sensitive surface absorption spectroscopy. In a theoretical analysis we showed that the sensitivity of fiber-based surface absorption spectroscopy can outperform free-beam techniques by several orders of magnitude. We applied our method to sub-monolayers of PTCDA molecules, deposited on the surface of an ultrathin fiber. The high sensitivity allowed us to record spectra with an excellent signal to noise ratio in a short time, revealing the dynamics of the deposition and of the post-

deposition evolution of the dilute molecular film on a second to minutes time scale. The experiments were carried out with an extremely simple and low-cost experimental set-up. Yet, the sensitivity of our measurements exceeded what was reached in previous studies by two orders of magnitude. Straightforward technical improvements should allow to further increase this value and to approach the ultimate sensitivity of the technique.

We wish to thank H. Giessen and Y. Louyer for their support in the early stages of the experiment and W. Alt, T. Fritz, and M. Hoffmann for valuable discussions. This work was supported by the EU (Research Training Network “FASTNet”) and the DFG (Research Unit 557).

* Present address: Institut für Physik, Universität Mainz, 55099 Mainz, Germany; Electronic address: rauschenbeutel@uni-mainz.de

- [1] V. Bordo and H.-G. Rubahn *Optics and Spectroscopy at Surfaces and Interfaces* (Wiley-VCH, Weinheim 2006)
- [2] Ph. H. Paul and G. Kychakoff, *Appl. Phys. Lett.* **51**, 12 (1987).
- [3] A. Messica, A. Greenstein, and A. Katzir, *Appl. Opt.* **35**, 2274 (1996).
- [4] Xh. Fang and W. Tan, *Anal. Chem.* **71**, 3101 (1999).
- [5] S. Simhony, I. Schnitzer, A. Katzir, and E. M. Kosower, *J. Appl. Phys.* **64**, 3732 (1988).
- [6] R. A. Potyrailo, S. E. Hobbs, and G. M. Hieftje, *Fresen. J. Anal. Chem.* **362**, 349 (1998).
- [7] B. D. Gupta, H. Dodeja, A. K. Tomar, *Opt. Quant. Electron.* **28**, 1629 (1996).
- [8] H. Tai, H. Tanaka, and T. Yoshino, *Opt. Lett.* **12**, 437 (1987).
- [9] J. Lou, L. Tong and Z. Ye, *Opt. Express* **13**, 2135 (2005).
- [10] M. D. Marazuela and M. C. Moreno-Bondi, *Anal. Bioanal. Chem.* **372**, 664 (2002).
- [11] H. Proehl, Th. Dienel, R. Nitsche, and T. Fritz, *Phys. Rev. Lett.* **93**, 097403 (2004).
- [12] F. Le Kien, J. Q. Liang, K. Hakuta, and V. I. Balykin, *Opt. Commun.* **242**, 445 (2004).
- [13] S. R. Forrest, *Chem. Rev.* **97**, 1793 (1997).
- [14] T. A. Birks and Y. W. Li, *J. Lightw. Tech.* **10**, 432 (1992).
- [15] J. D. Love and W. M. Henry, *Electron. Lett.* **22**, 912 (1986).
- [16] S. R. Forrest and Y. Zhang, *Phys. Rev. B* **49**, 11297 (1994).
- [17] The absorption cross section of PTCDA was calculated from the molar extinctions coefficient ϵ of PTCDA in solution [M. Hoffmann *et al.*, *Chem. Phys.* **258**, 73 (2000)] according to $\sigma = 2.303/N_A \times \epsilon$. We note that the averaged σ on the fiber may differ from the value obtained in solution by a factor of the order of one due to geometric reasons and differences in the refractive indices.
- [18] H. Proehl, R. Nitsche, Th. Dienel, K. Leo, and T. Fritz, *Phys. Rev. B* **71**, 165207 (2005).
- [19] The offset accounts for the fact that spectrum *B* still contains a monolayer component and thus an admixture of spectrum *A*.